International Journal of Heat and Mass Transfer 70 (2014) 23–32

Contents lists available at ScienceDirect

International Journal of Heat and Mass Transfer

journal homepage: www.elsevier.com/locate/ijhmt

Stable and uniform heat dissipation by nucleate-catalytic nanowires for boiling heat transfer

Beom Seok Kim, Sangwoo Shin, Donghwi Lee, Geehong Choi, Hwanseong Lee, Kyung Min Kim, Hyung Hee Cho *

Department of Mechanical Engineering, Yonsei University, 50 Yonsei-ro, Seodaemun-gu, Seoul 120-749, Republic of Korea

ARTICLE INFO

Article history:
Received 6 June 2013
Received in revised form 23 October 2013
Accepted 23 October 2013
Available online 16 November 2013

Keywords:
Boiling heat transfer
Heat transfer uniformity
Silicon nanowires
Nucleation dynamics
Capillary pumping
Cooling technology

ABSTRACT

Boiling-favorable merits of nanowire arrays are discussed for the thermal stability of boiling heat transfer. Local and temporal heat transfer characteristics are evaluated on vertically aligned nanowire arrays using a devised temperature-array sensor. The effects of rough morphology and highly wetting characteristics of nanowires lead to the reliable heat transfer stability/uniformity as well as efficient heat dissipation performances in pool boiling environments. The easy re-wetting and by-productive cavity-like structures via long nanowires can stabilize nucleation dynamics that catalyzes bubble nucleation dispersely and detaches developed bubbles quickly. Nanowires-inspired boiling heat transfer can make a breakthrough in improvements of heat transfer uniformity/stability with spatial and temporal temperature variations less than 1.0 and 2.0 K, respectively. SiNWs can also guarantee enhancements of both heat dissipation capacity and efficiency by more than 100% compared to a plain surface.

1. Introduction

Most of power generation systems from conservative fossil fuel-based systems to next-generation systems including thermoelectric and nuclear fusion systems, are based on sufficient absorption/isolation of thermal energy and efficient conversion from thermal to electric energy [1–3]. Especially for nuclear fusion reactor systems, blanket and divertor components should be exposed to huge amount of heat flux of 1–5 MW m^{-2} which is transferred from central high-temperature plasma in Tokamak system [4,5]. For realizing nuclear fusion plants as well as increasing the efficiency of conventional power plants, it is absolutely essential to increase and/or isolate operating temperatures in the system and stabilize thermal conditions of configuration components [6,7]. Locally concentrated thermal loads will finally cause thermal stress and fatigue which are principal reasons for the fatal failure of surfaces. Therefore, effective cooling technologies assuring stability of local/temporal thermal characteristics should be applied to cool the devices by releasing concentrated thermal load. One of the promising cooling technologies is a boiling heat transfer, which is based on the phase-change phenomena accompanying heterogeneous nucleation of liquid coolant, particularly for extremely high heat dissipating performance [8–10].

For boiling heat transfer, ultimate goals are to maximize allowable limit of heat dissipation capacity (or critical heat flux, CHF) and increase heat dissipation efficiency (or heat transfer coefficient, HTC) which are depicted by B and local differential on a curve from A to B in Fig. 1a, respectively. In addition, it would be necessary to reduce thermal loads required for the onset of nucleate boiling (ONB), which represents a starting point accelerating heat dissipation accompanying phase-change of liquid coolant compared to single-phase heat transfer of the coolant. Much effort has been devoted to demonstrating principal mechanisms of thermal energy dissipation through boiling heat transfer and improving the performances. Surface morphology and wettability characteristics, which are mutually related [11–15], are two principal factors determining the performances [16–20]. As depicted in Fig. 1b, the surface roughening greatly increases the interfacial area in contact with the working fluid (cooling agent) for heat transfer, and helps readily dissipate thermal energy toward the outer environment. In addition, it has been proved that the structures can facilitate the nucleation of coolant. Macro- and micro-scale artificial structures such as cavities, pin–fin arrays, and porous structures, have been typically used to modify surface morphology to catalyze the heterogeneous nucleation [21–24]. Moreover, highly wettable characteristics of surfaces are favorable to enhance the capacity of thermal energy dissipation by increasing accessibility of coolant towards the boiling surface [25–29].

* Corresponding author. Tel.: +82 2 2123 2828; fax: +82 2 312 2159.
E-mail addresses: kimmbs@yonsei.ac.kr (B.S. Kim), klui24@yonsei.ac.kr (S. Shin), donghwi84@yonsei.ac.kr (D. Lee), or50341@yonsei.ac.kr (G. Choi), lynm@yonsei.ac.kr (H. Lee), kimkm@yonsei.ac.kr (K.M. Kim), hhcho@yonsei.ac.kr (H.H. Cho).

0017-9310/$ - see front matter © 2013 Elsevier Ltd. All rights reserved.
http://dx.doi.org/10.1016/j.ijheatmasstransfer.2013.10.061

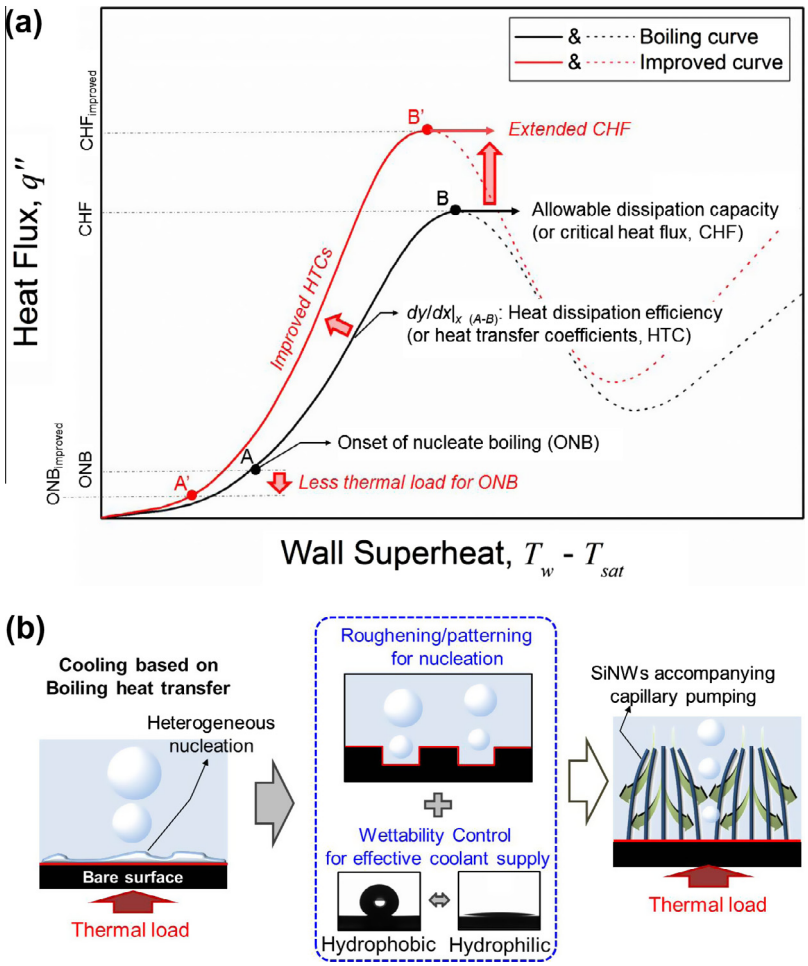

Fig. 1. Boiling heat transfer for efficient cooling technology. (a) Typical boiling curves representing performance factors including allowable heat dissipation capacity, heat dissipation efficiency, and onset of nucleate boiling. (b) Schematics of principal factors for the enhancement of boiling heat transfer and the merits of nano-structures on boiling applications.

Nano-structures such as nanorods and nanowires can fulfill the hydro-physical requirements to realize innovative enhancement of thermal energy dissipation based on boiling heat transfer [26,30–34]. It has been proved that extremely rough surface morphologies of nano-structures can lead to strong capillary pumping characteristics due to hemi-wicking phenomena based on Wenzel's model on wettability [14,35]. Based on this merit of nano-structures for boiling application, we present that nanostructural surface modifications can be a promissing solution to make breakthrough in the capacity and the efficiency of thermal energy dissipation as well as stability of local/temporal heat transfer characteristics for practical cooling systems. By experimental and analytical approaches of pool boiling using deionized (DI) water as a coolant, we verify that the improvements are attributed to reinforcing the coolant supply toward a interfacial solid surface and catalyzing the heterogeneous nucleation of saturated vapor easily. It will also be discussed that nucleation dynamics is strongly dependent on the surface morphology and wettability characteristics which are controlled via silicon nanowire arrays (SiNWs). In particular, we present that the geometrical control of nano-structures related to the formation of microscale by-productive cavities could be a crucial factor for controlling nucleative boiling characteristics, and it can contribute further enhancement of boiling performances.

2. Material and methods

2.1. Local heat transfer measuring sensor

For local and temporal boiling characterizing, we devise a temperature array sensor with SiNWs *in situ* on a silicon substrate as shown in Fig. 2. The sensor chip for measuring local temperatures and supplying heat fluxes consists of five sets of 4-wire resistance temperature detector (RTD) and a thin-film heater. Heat transfer area ($0.5 \times 1.0\ cm^2$) is designed at the center of the chip and the RTDs are arranged in at regular intervals of 1.5 mm. Signal accuracy and reliability of wall temperature can be exceptional due to the precise installation of the array sensor on a boiling surface in contact with working fluid. The sensor response time is calculated to be much less than the bubble generation frequency, which is in the order of tens of to hundreds of hertz.

A p-type silicon wafer (Boron-doped, (100) orientation, with a resistivity between 1 and 20 Ω cm) with the thickness of 500 μm is used as a substrate. The wafer is first cleaned for more than 40 min in a 1:3 mixture of H_2O_2 and H_2SO_4 by volume. The wafer is then further cleaned with acetone and methanol for 5 min each in turn. After the cleaning process, a photoresist (PR) coating is applied using a spin coater to spread it uniformly on the substrate

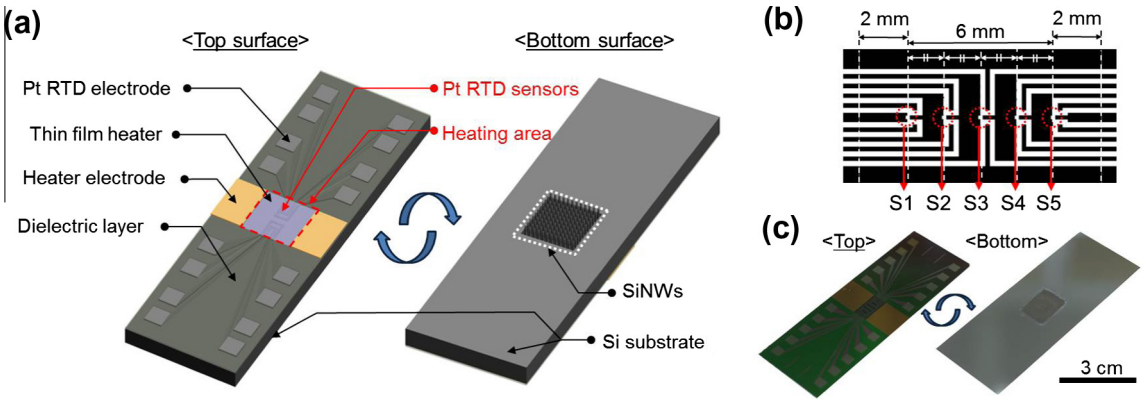

Fig. 2. The sensor chip with synthesized SiNWs *in situ* on a silicon substrate. (a) Schematics of RTD array sensors with SiNWs partially synthesized on the rear side of the heater. Whole heating area is 1.0 cm by 0.5 cm. (b) 5 RTD sensors in a row with the constant distance of 1.5 mm between each other. The RTDs are marked by S1, S2, S3, S4 and S5 in turn (from left to right). (c) Fabricated sensor chip corresponding to the schematics presented in (a).

and a hot plate to solidify it. Ultraviolet lithography is used to dissolve the PR selectively where RTDs would be formed. Platinum is deposited on the substrate, and the PR layer under the platinum is removed by a platinum lift-off process. An insulating layer of an oxide/nitride/oxide multilayer stack is deposited between the RTDs and a heater before forming the heater layer. The next step is to remove the insulating material deposited on the area of the RTD electrodes by an additional photolithography and a reactive ion etching. An indium tin oxide (ITO) layer is deposited and patterned by wet etching using a PR masking process to form the heater. Finally, gold electrodes are formed on both sides of the heater using an additional metal lift-off process.

2.2. Modification of surface morphology and wettability via SiNWs

Top-down metal-assisted chemical etching method (MaCE) is used to synthesize SiNWs [36,37]. This requires immersing each silicon piece in etching solution (a mixture of 5 M HF and 0.02 M $AgNO_3$) at room temperature. During the etching, Ag^+ ions dissolved in the solution attach themselves to the silicon surface by galvanic displacement [38]. The silicon surface in contact with the Ag^+ ions undergoes oxidization, and then the locally formed oxides are etched by the hydrofluoric acid. As the etching progresses, the remaining parts of silicon form vertical SiNWs. The etched silicon substrate is cleaned using nitride acid solution to remove the Ag dendrite structures [39]. Finally, the substrates with SiNWs are immersed in plenty of deionized (DI) water to rinse them, and then they are allowed to dry by natural convection under ambient conditions. For the synthesis of SiNWs on the completed sensor, we used Teflon holder with O-rings which prevents direct contact between the sensor and the etching solution except the rear side of the sensor via a rectangular etch-hole.

Based on inherent hydrophilic characteristics of a Si wafer with apparent contact angle (CA) about 43°, hydrophilicity can be enhanced by controlling the structural dimensions of SiNWs [14]. Based on our previous study, the critical height of SiNWs for superhydrophilic states was derived like $h_c \geq (1/\pi d)(1/\cos\theta^* - 1)(1-\varphi)(a+d)^2$ where h_c, d, θ^*, a, and φ represent the demanded height of SiNWs for superhydrophilicity, diameter of SiNWs, equilibrium CA on an ideal plain Si surface, distance between SiNWs, and solid fraction remaining dry ($\varphi = \pi d^2/\lfloor 4(a+d)^2 \rfloor$), respectively, under the assumption for circular pillar structures describing SiNWs. The height of SiNWs with the diameter d_{avg} = 100 nm and distance between SiNWs a_{avg} = 200 nm, which are determined by SEM images, should be longer than 2-μm for a superhydrophilic surface [14]. Based on this pre-conditioning analysis, we synthesize SiNWs with the average heights of 2- and 15-μm using etching times of 10 and 70 min, respectively. These two cases will be compared presenting boiling performances affected by the morphological variation of SiNWs regardless of the wettability characteristics.

2.3. Quantification of bubble dynamics

Detaching bubble characteristics are analyzed using a visualization system. Quantitative results of the frequency and mean radius of bubbles are analyzed by a software, Dynamic studio 3.30 (Dantec Dynamics). The mean radius of detaching bubbles presents the identical mean radius of bubbles by assuming that the bubbles can be treated as completely spherical ones.

3. Experimental

3.1. Pool boiling experiments

Fig. 3 shows a schematic diagram of pool boiling experimental facilities. The chamber is made of stainless steel. Two immersion

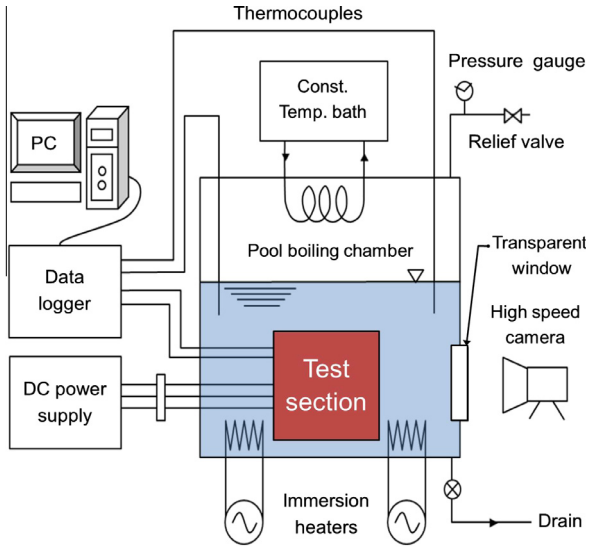

Fig. 3. Schematic diagram of the pool boiling experimental facility for the installation of the fabricated sensor [29]. This figure is reprinted with permission from AIP.

heaters and a relief valve with a pressure gauge are attached to the chamber to control experimental conditions. There are transparent windows made of tempered glass in the sidewall of the chamber. Two K-type thermocouples are inserted in the chamber at different heights to measure the temperature of the working fluid. A coil-type heat exchanger (condenser) in the upper part of the chamber is connected to a constant-temperature bath. A 200 V-10 A power supply (KSC Korea Switching, Korea) is used to supply the heat flux. Voltage drops and currents are measured across the thin-ITO heater and a shunt which is inserted in the electric circuit, respectively. These signals are acquired by a data logger (34970A, Agilent Technologies) and then processed by a computer. The resistance values from the RTDs are measured by a data acquisition module (SCXI-1503, National Instruments) connected to a digital acquisition board (PCI-6259, National Instruments). A high-speed camera (pco.4000, PCO) is employed to visualize the nucleated behavior of bubbles. For the installation of the sensor, the main body of test section is made of Teflon with low thermal conductivity (k_{teflon} = 0.23 W m^{-1} K^{-1}) to minimize heat conduction loss. Spring probes and electric busbars (Cu) are arranged for acquiring temperature-dependent resistance signals from the RTDs and applying electric currents through the ITO heater, respectively. The portion of the test section just below the installed sensor and a cover plate are made of macerite ceramic SP ($k_{macerite}$ = 1.6 - W m^{-1} K^{-1}) with a melting point higher than 1000 °C to prevent conductive heat loss and breakdown when test conditions approach the CHF limitation. The gap between the sensor and the test section is sealed using room-temperature vulcanization silicone (RTV Ultra Blue – 77BR, Permatex) along the edge of the cover plate.

We use DI water as a working fluid under the saturated condition (T_{sat} = 100°C) at an atmospheric pressure. Experiments are conducted after removing gases dissolved in the reserved DI water. After making steady-state conditions at a controlled heat flux value, all of the data including wall temperatures from the RTDs are taken for more than 30 s. The resistance signals for evaluating wall temperature are monitored with the frequency of 1000 Hz.

3.2. Data reduction process [40]

3.2.1. Surface wall temperature

The wall temperature can be calculated to indicate surface temperature based on the location of the RTDs, which are on the bottom of the sensor chip. It is possible to derive the surface wall temperature from Fourier's law for thermal conduction as follows:[41,42]

$$T_w = T_R - \frac{1}{k_{Si}} \cdot q'' \tag{1}$$

where T_R, l, k_{Si}, q'', and T_w represent the temperature measured by the RTDs on the bottom of the installed sensor chip, characteristic length for a distance in the heat flow direction (i.e. the Si substrate thickness), thermal conductivity of the Si substrate ($k_{Si} \sim 140$ W m^{-2} K^{-1}), heat flux, and surface wall temperature on the top surface close to the working fluid, respectively. We assume that the Si substrate of the sensor chip is sufficiently thin (500 μm) for one-dimensional heat conduction due to its own high thermal conductivity.

3.2.2. Local heat transfer coefficient

It is necessary to evaluate local convective heat transfer coefficients on boiling surfaces. This allows us to quantify the cooling performance on boiling heat transfer due to the temperature difference induced by buoyancy force, bubble nucleation/detachment from a heated surface and refreshing of liquid-phase working fluid towards the boiling surface. According to Newton's law of cooling,[41,42] the convective heat transfer coefficient h can be expressed as

$$h = q''/(T_w - T_f) \tag{2}$$

where T_w and T_f are the wall temperature from Eq. (1) and liquid-phase fluid temperature ($T_{sat} = T_{fluid,\infty}$ = 100 °C), respectively. Derivation of the local heat transfer coefficient is based on the temperature deviation between the local wall temperature from each RTD and measured bulk temperature of the working fluid in the experimental boiling chamber.

3.2.3. Critical heat flux

When heat flux approaches CHF points, local wall temperatures fluctuate significantly with abrupt temperature increase. It is because vaporized bubbles accompany the coalescence of separate vapor bubbles and then form a thin film layer which insulates heat dissipation from a solid to liquid coolant. Herein, the heat flux value of CHF is determined by adding the heat flux measured at a certain point which shows the significant fluctuation or increase (more than 15 degrees of centigrade) and a half of increment from the measured heat flux which has been measured as the previous step.[40]

3.3. Uncertainty analyses

All errors are estimated with a confidence level of 95% with sufficient measured data for each variable. The uncertainty analysis is performed not only for the variables related to the basic dimensional estimations, but also for the main variables described in the data reduction procedure presented above. Errors for dimensional estimation of the sensor and for temperature measurement by conventional thermocouples are 0.2% and 1.32 K, respectively. For the uncertainty of the applied heat flux, estimation of heat loss directly towards the outer environment is difficult due to complicated boundary conditions. Therefore, the loss is evaluated by three-dimensional numerical analyses using a commercial code (Fluent 6.3.26, ANSYS), comparing the results with the experimental results on wall temperature data. A local hot spot at the center of the heating surface is used to extract a representative temperature value at a specific heat flux condition (78.9 W cm^{-2}) for a plain Si surface. Herein, because the two-phase heat transfer coefficient cannot be directly measured, the initial boundary condition is based on the experimental results [43]. By varying the heat transfer coefficient, the surface temperature is adjusted iteratively to achieve a deviation less than 1.0% compared to the experimental value. With this condition satisfied, the heat flux outwards from the heater surface is compared to the input heat flux. Based on the relationships used to derive the variables such as $(\delta q''/q'') = [(\delta V/V)^2 + (\delta I/I)^2 + (\delta A/A)^2 + (\delta q''_{loss}/q''_{actual})^2]^{1/2}$,[44] the estimated uncertainty of the applied heat flux is 6.4%. The same procedures using related variables give uncertainties of surface wall temperatures and local heat transfer coefficients of 6.4% and 6.5%, respectively.

4. Results and discussion

4.1. Spatial and temporal heat transfer uniformity

Fig. 4 shows time-averaged spatial wall temperature distributions according to different heat flux conditions. We can see that SiNWs could cool the entire heated surface down with wall superheating less than 40.0 K, and remarkably enhance temperature uniformity within 1.0 K with the spatial standard deviation of 0.61 K for 15-μm SiNWs at an allowable maximum heat flux conditions. On the plain surface, after the nucleation of coolant at high

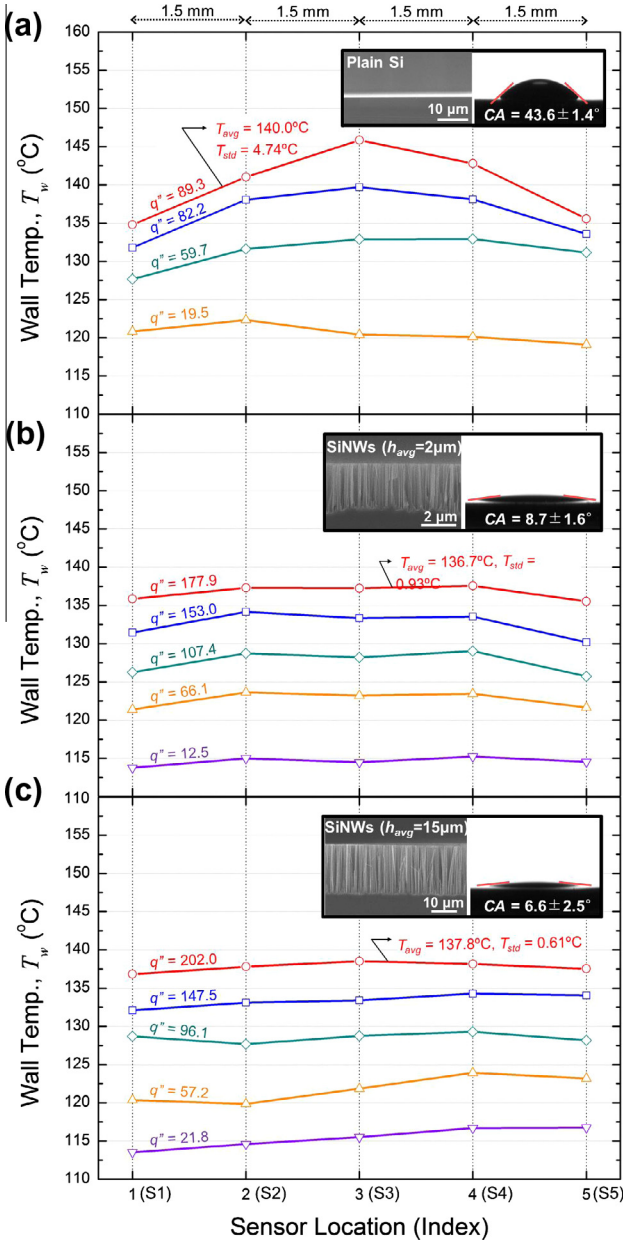

Fig. 4. Evaluation of spatial temperature uniformity (a) for a plain Si surface, (b) for a surface with 2-μm SiNWs, and (c) for a surface with 15-μm SiNWs. Insets present cross-sectional morphology taken by FE-SEM and static contact angle for a plain surface, and surface with SiNWs of 2- and 15-micron height, respectively.

heat flux conditions, we can see that there are significant local temperature differences by more than 11.0 K even in the short lateral distance (3 mm) from the center to the outside area. Temperature in the center region at heat flux of 89.3 W cm^{-2} exceeds 145.8 °C with spatial standard deviations of 4.7 K. Comparing to the plain surface, central temperature at much higher heat flux conditions greatly decreased by 8.6 and 7.3 K for 2- and 15-μm SiNWs, respectively. Furthermore, the whole heat flux conditions for both surfaces with 2- and 15-μm SiNWs have remarkably reduced spatial temperature gradient without any notable peaks on the graphs. From these results, we can present that the surfaces with SiNWs can guarantee uniform wall temperatures with spatial standard deviation less than 1.0 K. This means that SiNWs in boiling heat transfer are highly effective for the releasing of local concentration of thermal load under harsh thermal dissipating environments.

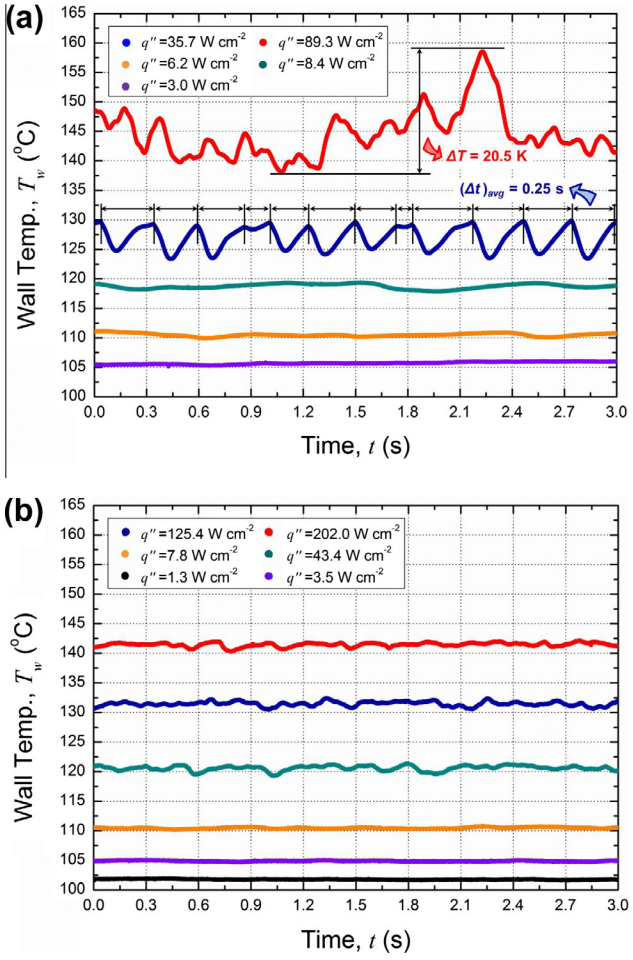

Fig. 5. Transient surface temperature variations in the center area (S3) according to heat flux variations for (a) a plain Si surface, and (b) a surface with 15-μm SiNWs.

Temporal variations of local wall temperature from a local measuring point of S3 are presented in Fig. 5. For the plain surface, when the heat flux exceeds onset of nucleation boiling point (ONB), temperature fluctuations with regular amplitude and nearly constant period are observed due to the discrete bubble nucleation and detachment with the growth period of about 0.25 s (at q'' = 35.7 W cm^{-2} in Fig. 5a). As heat flux approaches CHF, irregular and abnormal temperature fluctuations occur with much higher instantaneous deviations greater than 20 K. A thermal insulating vapor layer (thermal conductivity of water vapor ~ 0.016 W m^{-2} K^{-1}) by the coalescence of developed bubbles on a heating surface prohibits heat dissipation towards coolant and then this results in the abrupt temperature increase, which will finally cause surface failure. The considerable temporal fluctuation with high amplitude and the abnormal temperature fluctuation will decrease the surface stability under cooling applications and cause critical thermal failures due to thermal fatigue by repeated thermal stress under long-term boiling application. However, the local mid-point of the surface with SiNWs does not show any significant temporal temperature fluctuations for whole heat flux conditions (Fig. 5b). Particularly, on a surface with SiNWs of 15-μm high, the amplitude of the temperature fluctuations are less than 2.0 K without any abnormal peaks even at a heat flux condition up to 202.0 W cm^{-2}. It can be presented that SiNWs have innovative merits for suppressing temporal wall temperature fluctuations without any remarkable vibrations under boiling heat transfer. The significant local/temporal temperature deviations as well as the irregular abnormal

overheating can be prevented by SiNWs-employed surfaces and, therefore, it helps stabilizing thermal energy dissipations uniformly and constantly. From these immediate results, the application of SiNWs can be powerful to improve the thermal stability of boiling heat transfer.

4.2. Nucleation characteristics: demonstrations and effective model

These spatial and temporal thermo-physics could be demonstrated based on nucleation dynamics dominated by surface manipulation conditions related to both roughness and wettability characteristics. In nucleate boiling regime on the plain surface, vaporized-bubbles are intensively generated on the middle of the heating area as presented in Fig. 6a–c. Large bubbles are densely nucleated and detached repeatedly, and then they cause the considerable local temperature deviation accompanying temperature increase especially on the center area as discussed above in Fig. 4a. The local temperature must be increased where the vapor bubbles generate intensively because the superheated vapor bubbles prevent the surface from contacting the liquid-phase fresh working fluid. On the other hand, we can see that incipient bubbles are getting smaller (Fig. 6d and g) on surfaces with SiNWs compared to the plain Si surface with the bubble diameter of about a few millimeters. This can be explained by the superhydrophilicity and the highly disordered surface morphology with lots of natural cavities induced by the vertically aligned SiNWs. Effective cavity sizes for nucleation can be decreased from tens of micron to even nanoscales according to increasing wall temperature by sufficient thermal energy. According to surface wettability characteristics, the effective cavity sizes for a given wall superheat can be expressed analytically as follows [45,46]:

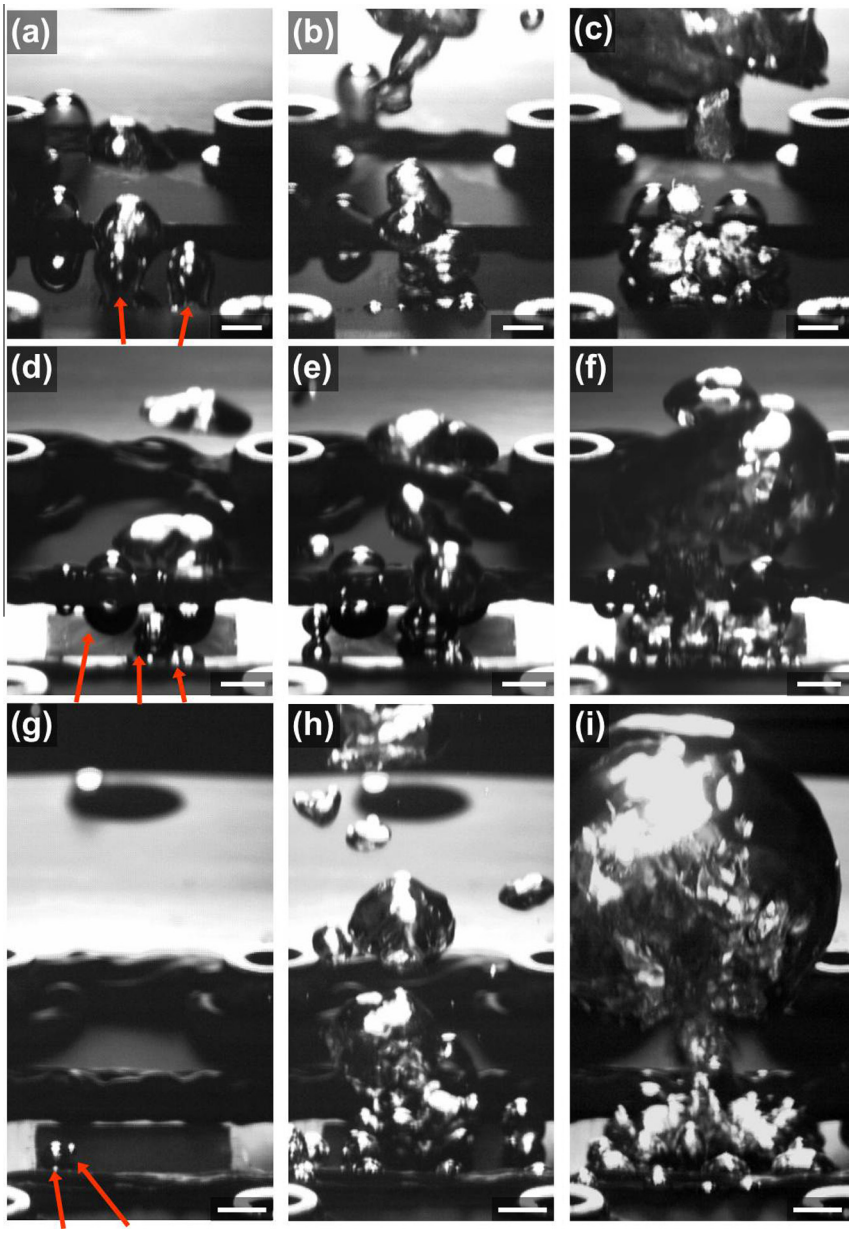

Fig. 6. Visualizations according to heat flux variations (a, b, c) on a plain Si surface at $q'' = 19.5, 45.4$, and 85.8 W cm^{-2}, respectively, (d, e, f) on a surface with 2-μm SiNWs at $q'' = 6.9, 50.0$, and 168.4 W cm^{-2}, respectively, and (g, h, i) on a surface with 15-μm SiNWs at $q'' = 4.3, 34.4$, and 202.0 W cm^{-2}, respectively. Scale bars are 3 mm and red arrows indicate discrete nucleation sites. Movies for each experimental from the plain and the surface with 15-μm SiNWs are available from SI. (For interpretation of the references to color in this figure legend, the reader is referred to the web version of this article.)

$$\begin{Bmatrix} r_{c,min} \\ r_{c,max} \end{Bmatrix} = \frac{\delta_t K_1}{2K_2}\left[1\begin{Bmatrix} - \\ + \end{Bmatrix}\sqrt{1-\frac{8K_2\sigma T_{sat}(P_l)}{\rho_v h_{fg}\delta_t T_{superheat}}}\right] \quad (3)$$

where δ_t, σ, $T_{sat}(P_l)$, ρ_v, h_{fg}, $T_{superheat}$ represent the thermal boundary layer thickness, surface tension of liquid, saturation temperature according to pressure of liquid, vapor density, latent heat of vaporization, and wall superheat ($T_w - T_{sat}$), respectively. Two constants $K_1 = \sin\theta$ and $K_2 = 1 + \cos\theta$ reflect surface wettability characteristics. Based on these relationships, we can deduce that superhydrophilicity via SiNWs induces the decrease of effective cavity sizes required for nucleation as shown in Fig. 7a. The vertically aligned SiNWs lead to morphologically favorable conditions as well as superhydrophilicity. SiNWs with high aspect ratio form naturally-induced beneficial cavities [26,47], therefore, these actual cavity structures in the range from hundreds of nanometers to a few micron can satisfy the prerequisites within the analytically estimated ranges for effective nucleation cavities. On the other hand, a smooth surface without any beneficial cavities requires great amount of wall superheat to meet the requirement for nucleation while waiting the range-extension of effective nucleation cavities. Due to the hydrophilic and rough surface conditions with actual cavities via SiNWs, two-phase boiling heat transfer can be advanced accompanying smaller bubbles under much lower wall superheat conditions. Consequently, heat flux is required by 19.5 W cm^{-2} for the starting of boiling heat transfer on a plain Si (Table 1). Meanwhile, the rough surfaces with SiNWs favor the nucleation of vapor bubbles with much lower heat flux and do not lead to excessive wall superheating before boiling incipience. We can verify that SiNWs are powerful to facilitate nucleative thermal energy dissipation by decreasing required thermal loads by 77.7% via 15-μm SiNWs. Wall superheats for the starting of nucleation were 13.2 and 5.1 K for 2- and 15-μm SiNWs, respectively, and these are significantly decreased compared to 31.1 K on the plain surface.

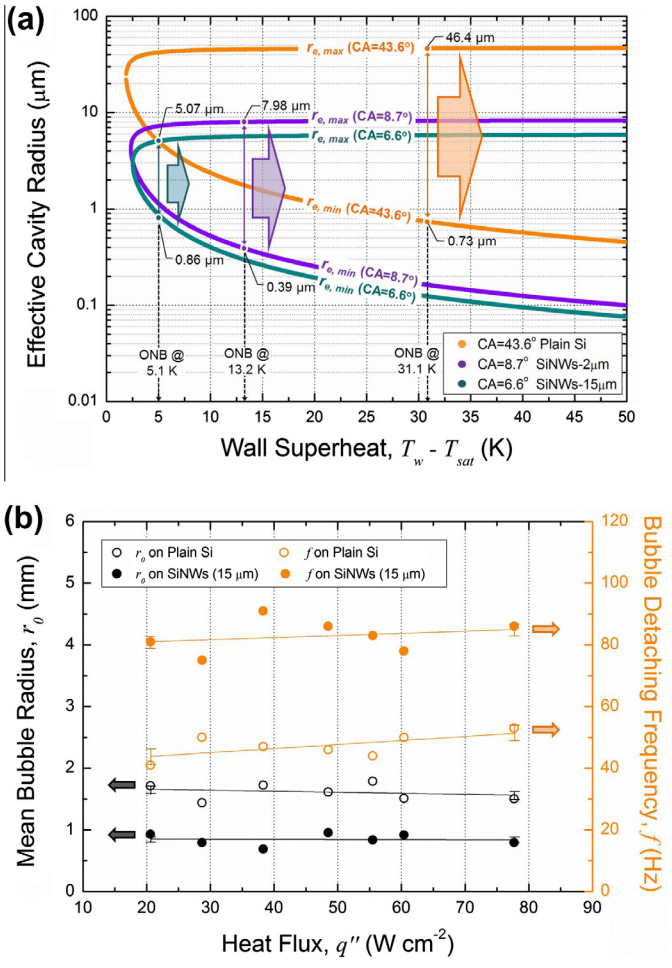

Fig. 7. Quantitative results on bubble dynamics. (a) Effective nucleation cavity radius according to wettability variations. Critical nucleative radiuses at ONBs estimated by the experiments are indicated for the range of effective cavity radius. (b) Mean radius of detaching bubbles and their frequencies on a plain and a surface coated by 15-μm SiNWs. Solid lines in each result are linear-fitted correlation curves.

We confirm that the departure frequency of fully-developed bubbles is much faster on the surface with SiNWs than that on the plain surface (Fig. 7b). The nucleated small bubbles conformable to the conditions via SiNWs would result in high frequency of bubble detachment. It was previously explained that the detaching frequency is dependent on surface wettability characteristics, and the more hydrophilic surfaces, the easier and the faster bubble detachment took place [27,30]. In particular, the detaching frequency, f can be in inverse proportion to the diameter of detaching bubbles as follows [48,49]:

$$(2r_0)\cdot f = 0.59\left[\frac{g^2\sigma(\rho_l-\rho_v)}{\rho_l^2}\right]^{0.25} \sim Constant \quad (4)$$

where r_0, g, and ρ_l mean the radius of detaching bubble, gravitational acceleration and density of liquid, respectively. In Eq. (4), right term could be treated as constant because it is composed of physical properties. As presented in Fig. 7b, small bubbles on a surface with SiNWs are detaching much faster than those on a plain surface. Herein, the separately detaching small bubbles with high departure frequency would allow large spatial and temporal vacant area between the bubbles that enable a direct contact with the surface of the liquid-phase working fluid. These physical characteristics on spatial and temporal bubble behaviors, which decreases re-wetting friction combined with hydrophilic nature, can be a principal ground for less local temperature deviation and decrease of overall temperature on SiNWs surface compared to a plain surface with the slow nucleation and detachment of large bubble. Even though fully-developed bubbles finally give rise to surface dryout as the heat flux comes close to CHF, the distributed nucleating/detaching bubbles with small size and the favorable rewetting characteristics due to SiNWs can cool the boiling surface more effectively and then it would result in the stable thermal energy dissipation with improved spatial temperature uniformity and less temporal thermal fluctuations.

Due to the phase-change of the liquid coolant, the nucleated bubbles become more superheated than the liquid-phase working fluid, which maintains the saturated temperature (100 °C) at atmospheric pressure. The superheated vapor bubbles with low density will rise up from nucleated sites after the fully-development. On a plain surface, however, the large bubble size and the relatively slow detachment take place in the center area intensively. It can be deduced that the working fluid maintaining lower temperature compared to the superheated vapor bubbles induces more effective cooling on the outside region of the heat transfer surface by direct contact with the surface without any obstructions such as the thermal insulating vapor layer. In other words, the outside region could keep low surface temperature than the center region due to the merit of better accessibility of liquid-phase cooling agent by relatively low re-wetting friction [50,51]. Contrary to the large bubbles from a plain surface, the discretely distributed small bubbles from a surface with SiNWs would cause the decrease of local re-wetting resistance allowing easy access of working fluid toward the heating surface. The liquid on hydrophilic surface (CA < 90°) has to satisfy the Young–Laplace equation such as $z_i = \sigma\cos\theta/(\rho_l-\rho_v)ga_{avg}$, where z_i is the equilibrium height of permeated liquid between SiNWs due to capillary force. Based on this relationship densely

Table 1
Quantitative heat flux values for ONB and CHF with measured wall temperatures according to the surface manipulation conditions.

	Onset of nucleate boiling		Critical heat flux		
	q''_{ONB} (W cm^{-2})	T_w (°C)	q''_{CHF} (W cm^{-2})	T_w (°C)	$q''_{CHF}/q''_{CHF,plain}$
Plain	19.5	131.1	90.2	145.8	1.0
2-μm SiNWs	9.4	113.2	179.6	137.2	1.99
15-μm SiNWs	4.4	105.1	203.2	138.5	2.25

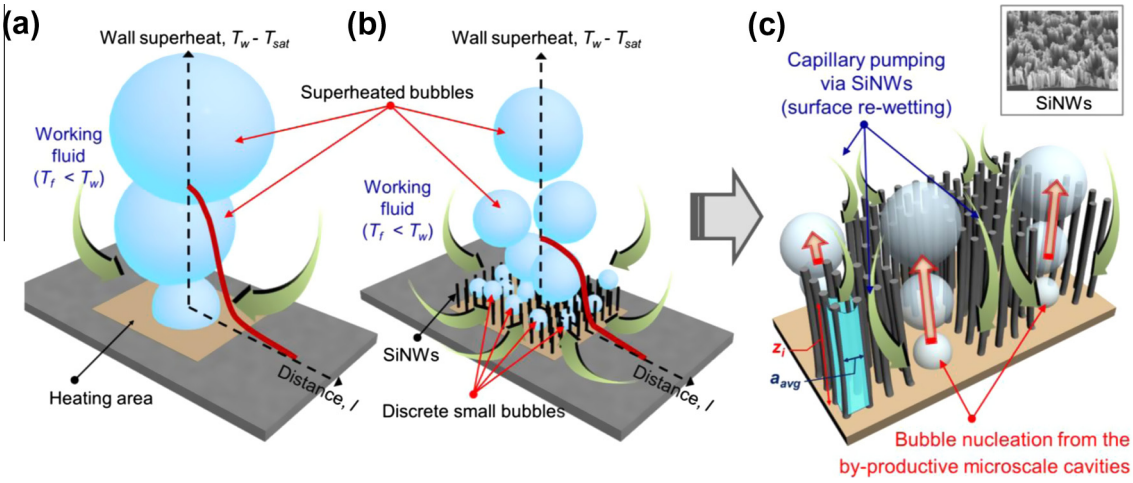

Fig. 8. Nucleation dynamics and its effect on heat transfer characteristics dependent on surface conditions on (a) a plain Si surface and (b) a surface with SiNWs. (c) Capillary pumping effect via SiNWs and nucleated bubbles by the by-productive microscale cavities conformable to the effective cavity sizes. Inset of (c) presents SEM images for SiNWs and the cavity-like vacancy area.

distributed SiNWs with small distance of a_{avg}, can induce by for higher z_i compared to a plain surface condition. Consequently, dispersed nucleation with small size and high detaching frequency may reduce the local re-wetting friction even on the center region by widening spatial and temporal vacant space for the coolant supply, and therefore the surface with SiNWs can dissipate heat evenly and effectively. These can lead to better uniformity of thermal characteristics on the entire heat transfer surfaces and improved heat dissipation efficiency/capacity all together. Fig. 8 schematically present the physics of nucleation dynamics according to the application of SiNWs and explain the merits of SiNWs with respect to the stable and the improved thermal energy dissipation through boiling heat transfer.

4.3. Enhancement of boiling heat transfer performances

The bubble dynamics and consequent heat transfer performances are characterized into boiling curves and HTCs to present heat dissipation capacity and efficiency, respectively, as shown in Fig. 9a and b. From Fig. 9a we can see that heat dissipation capacity (i.e. CHF) and heat transfer efficiency (i.e. HTC) are significantly improved by the application of SiNWs. CHFs are remarkably improved by 99.1% and 125.3% compared to the plain surface via SiNWs with the height of 2 and 15 μm, respectively. The highly wettable surfaces can lead to the extension of CHF because they enhance water-accessibility towards a boiling surface to retard surface dryout against drastic nucleation [26,27,30]. In addition, maximum HTCs on a central hot spot (at S3) are increased by 125.7% (47,400 W m^{-2} K^{-1}) and 149% (52,300 W m^{-2} K^{-1}) via 2- and 15-μm SiNWs, respectively. Herein, we can find differences on boiling performances between long (15-μm) and short (2-μm) SiNWs. As presented in Table 1, CHF for the long SiNWs (203.2 W cm^{-2}) is up to 13.1% higher than that of the short SiNWs (179.6 W cm^{-2}). In addition, ONB for the short SiNWs requires more thermal energy by 5.0 W cm^{-2} than that of high SiNWs. However, both manipulated surfaces show sufficient superhydrophilic wettability with apparent CAs less than 10° [14]. Because there are few differences on apparent CAs between the two cases, we can infer that the performance disparities are strongly dependent on morphological surface characteristics under the confined water-favorable conditions. Insets of Fig. 9b present the geometrical differences between the surfaces with 2- and 15-μm SiNWs, respectively. When the vertical SiNWs with high aspect ratio are densely distributed, they tend to mutually conglomerate due to van der Waals force [47]. They then form the relatively large cavity-like vacant areas up to tens of microns across. More and larger microscale cavities exist on the surface with the long SiNWs compared to that with the short SiNWs. As heat flux and wall superheat increase, these areas can act as the actual cavities for vapor seeds to promote vapor nucleation and detachment in the non-conglomerated regions while the forests of SiNWs are attracting waters by the capillary pumping characteristics. The previous analytical approaches predicting the effective cavity radius on nucleate boiling showed that boiling heat transfer can be augmented by the existence of wider ranges of microscale cavities according to the increase of wall superheat [26,30,45]. Therefore, we can demonstrate that higher SiNWs with high aspect ratios (h/d_{avg}), which result in larger and more cavity-like structures, would be a critical factor for further improvement of boiling performance accompanying advanced ONB and extended CHF with higher HTCs [52].

5. Conclusions

In this study, we present boiling-favorable merits of nanowire arrays for the thermal stability of boiling heat transfer. Local and temporal heat transfer characteristics are evaluated on vertically aligned nanowire arrays using a devised sensor. We demonstrated that the effects of rough morphology and capillary pumping characteristics of SiNWs lead to the reliable thermal stability and

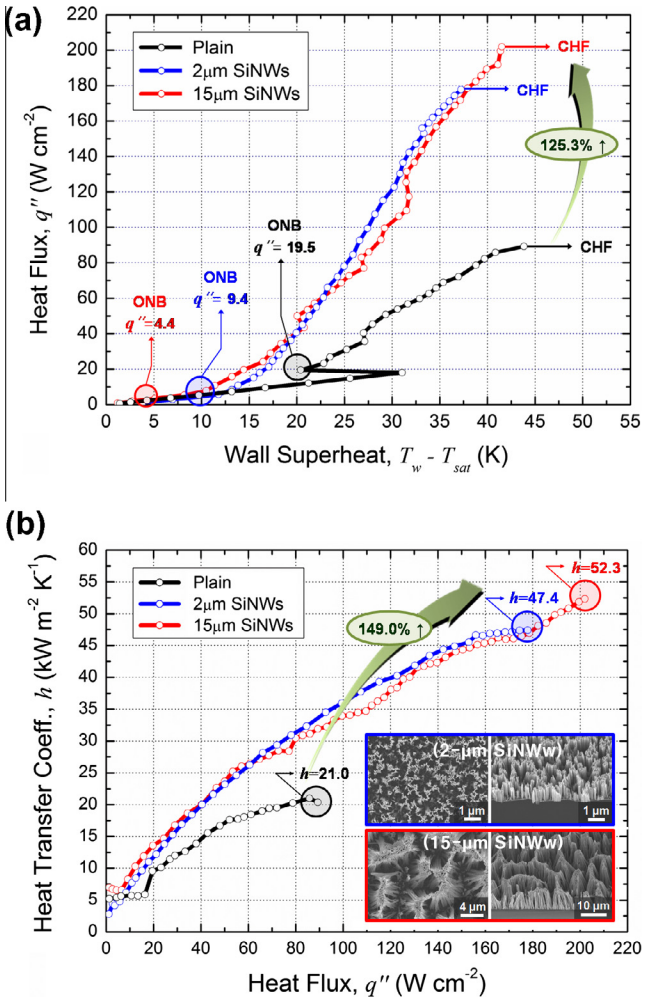

Fig. 9. Boiling performances for thermal energy dissipation capacity and efficiency. (a) Local boiling curves and (b) local heat transfer coefficients from central measuring point (S3) on each manipulated surface. Insets of (b) are surface morphology for 10-min etched silicon surface with short SiNWs (2 μm long), and for 70-min etched silicon (15 μm long) with conglomerated SiNWs forming natural microscale cavities.

efficient thermal energy dissipation in pool boiling environments. The easy re-wetting and by-productive cavity-like structures via SiNWs can lead to stabilized nucleation dynamics that catalyzes bubble nucleation dispersely and detaches developed bubbles quickly. As a result, nanowires-inspired boiling heat transfer can make a breakthrough in the improvements of heat transfer uniformity/stability with spatial and temporal temperature variations less than 1.0 and 2.0 K, respectively. SiNWs can also guarantee the enhancement of both heat dissipation capacity and efficiency by more than 100% compared to a plain surface. The height of nanowires, which affects the creation of by-productive nucleation sites within micron-scale, can be a crucial factor for heat dissipating improvements under superhydrophilic conditions. The results would be powerful to acquire its own value for a number of applications related to the thermal design of "Macro-systems" on energy harvesting systems, heating/cooling systems, power plants and so on in engineering fields.

Acknowledgments

This work was supported by a National Research Foundation of Korea (NRF) grant funded by the Korea government (MEST) (No. 2011-0017673) and the Human Resources Development program (No. 20134030200200) of the Korea Institute of Energy Technology Evaluation and Planning (KETEP) grant funded by the Korea government Ministry of Trade, Industry and Energy. The author B.S. Kim is grateful for a Seoul Science Fellowship provided by the Seoul Metropolitan Government.

References

[1] A. Bejan, Theory of heat transfer-irreversible power plants, Int. J. Heat Mass Transfer 31 (1988) 1211–1219.
[2] M. Zebarjadi, K. Esfarjani, M.S. Dresselhaus, Z.F. Ren, G. Chen, Perspectives on thermoelectrics: from fundamentals to device applications, Energy Environ. Sci. 5 (2012) 5147–5162.
[3] R.Z. Wang, R.G. Oliveira, Adsorption refrigeration – an efficient way to make good use of waste heat and solar energy, Prog. Energy Combust. Sci. 32 (2006) 424–458.
[4] M. Enoeda, Y. Kosaku, T. Hatano, T. Kuroda, N. Miki, T. Honma, M. Akiba, S. Konishi, H. Nakamura, Y. Kawamura, S. Sato, K. Furuya, Y. Asaoka, K. Okano, Design and technology development of solid breeder blanket cooled by supercritical water in Japan, Nucl. Fusion 43 (2003) 1837–1844.
[5] K. Tobita, S. Nishio, M. Enoeda, M. Sato, T. Isono, S. Sakurai, H. Nakamura, S. Sato, S. Suzuki, M. Ando, K. Ezato, T. Hayashi, T. Hirose, T. Inoue, Y. Kawamura, N. Koizumi, Y. Kudo, R. Kurihara, T. Kuroda, M. Matsukawa, K. Mouri, Y. Nakamura, M. Nishi, Y. Nomoto, J. Ohmori, N. Oyama, K. Sakamoto, T. Suzuki, M. Takechi, H. Tanigawa, K. Tsuchiya, D. Tsuru, Design study of fusion DEMO plant at JAERI, Fusion Eng. Des. 81 (2006) 1151–1158.
[6] K.V. Lobachyov, H.J. Richter, High efficiency coal-fired power plant of the future, Energy Convers. Manage. 38 (1997) 1693–1699.
[7] P. Chiesa, E. Macchi, A thermodynamic analysis of different options to break 60% electric efficiency in combined cycle power plants, J. Eng. Gas Turbines Power 126 (2004) 770–785.
[8] V.K. Dhir, Boiling heat transfer, Annu. Rev. Fluid Mech. 30 (1998) 365–401.
[9] B. Agostini, M. Fabbri, J.E. Park, L. Wojtan, J.R. Thome, B. Michel, State of the art of high heat flux cooling technologies, Heat Transfer Eng. 28 (2007) 258–281.
[10] M.A. Ebadian, C.X. Lin, A review of high-heat-flux heat removal technologies, J. Heat Transfer-Trans. ASME 133 (2011) 110801.
[11] A. Lafuma, D. Quere, Superhydrophobic states, Nat. Mater. 2 (2003) 457–460.
[12] F.C. Cebeci, Z.Z. Wu, L. Zhai, R.E. Cohen, M.F. Rubner, Nanoporosity-driven superhydrophilicity: a means to create multifunctional antifogging coatings, Langmuir 22 (2006) 2856–2862.
[13] D. Quere, Wetting and roughness, Annu. Rev. Mater. Res. 38 (2008) 71–99.
[14] B.S. Kim, S. Shin, S.J. Shin, K.M. Kim, H.H. Cho, Control of superhydrophilicity/superhydrophobicity using silicon nanowires via electroless etching method and fluorine carbon coatings, Langmuir 27 (2011) 10148–10156.
[15] Y. Coffinier, G. Piret, M.R. Das, R. Boukherroub, Effect of surface roughness and chemical composition on the wetting properties of silicon-based substrates, C. R. Chim. 16 (2013) 65–72.
[16] H.M. Kurihara, J.E. Myers, The effects of superheat and surface roughness on boiling coefficients, AIChE J. 6 (1960) 83–91.
[17] S.G. Kandlikar, A theoretical model to predict pool boiling CHF incorporating effects of contact angle and orientation, J. Heat Transfer-Trans. ASME 123 (2001) 1071–1079.
[18] O.C. Thomas, R.E. Cavicchi, M.J. Tarlov, Effect of surface wettability on fast transient microboiling behavior, Langmuir 19 (2003) 6168–6177.
[19] I.L. Pioro, W. Rohsenow, S.S. Doerffer, Nucleate pool-boiling heat transfer. I: review of parametric effects of boiling surface, Int. J. Heat Mass Transfer 47 (2004) 5033–5044.
[20] B.S. Kim, S. Shin, S.J. Shin, K.M. Kim, H.H. Cho, Micro-nano hybrid structures with manipulated wettability using a two-step silicon etching on a large area, Nanoscale Res. Lett. 6 (2011) 333.
[21] S.G. Liter, M. Kaviany, Pool-boiling CHF enhancement by modulated porous-layer coating: theory and experiment, Int. J. Heat Mass Transfer 44 (2001) 4287–4311.
[22] L. Zhang, M. Shoji, Nucleation site interaction in pool boiling on the artificial surface, Int. J. Heat Mass Transfer 46 (2003) 513–522.
[23] J.J. Wei, H. Honda, Effects of fin geometry on boiling heat transfer from silicon chips with micro-pin-fins immersed in FC-72, Int. J. Heat Mass Transfer 46 (2003) 4059–4070.
[24] H.S. Ahn, H.J. Jo, S.H. Kang, M.H. Kim, Effect of liquid spreading due to nano/microstructures on the critical heat flux during pool boiling, Appl. Phys. Lett. 98 (2011) 071908.
[25] H.T. Phan, N. Caney, P. Marty, S. Colasson, J. Gavillet, Surface wettability control by nanocoating: the effects on pool boiling heat transfer and nucleation mechanism, Int. J. Heat Mass Transfer 52 (2009) 5459–5471.
[26] R. Chen, M.C. Lu, V. Srinivasan, Z. Wang, H.H. Cho, A. Majumdar, Nanowires for enhanced boiling heat transfer, Nano Lett. 9 (2009) 548–553.
[27] A.R. Betz, J. Xu, H.H. Qiu, D. Attinger, Do surfaces with mixed hydrophilic and hydrophobic areas enhance pool boiling?, Appl Phys. Lett. 97 (2010) 141909.
[28] N.A. Patankar, Supernucleating surfaces for nucleate boiling and dropwise condensation heat transfer, Soft Matter 6 (2010) 1613–1620.
[29] S. Shin, B.S. Kim, G. Choi, H. Lee, H.H. Cho, Double-templated electrodeposition: simple fabrication of micro–nano hybrid structure by

electrodeposition for efficient boiling heat transfer, Appl. Phys. Lett. 101 (2012) 251909.
[30] C. Li, Z. Wang, P.I. Wang, Y. Peles, N. Koratkar, G.P. Peterson, Nanostructured copper interfaces for enhanced boiling, Small 4 (2008) 1084–1088.
[31] M.C. Lu, R.K. Chen, V. Srinivasan, V. Carey, A. Majumdar, Critical heat flux of pool boiling on Si nanowire array-coated surfaces, Int. J. Heat Mass Transfer 54 (2011) 5359–5367.
[32] D. Li, G.S. Wu, W. Wang, Y.D. Wang, D. Liu, D.C. Zhang, Y.F. Chen, G.P. Peterson, R. Yang, Enhancing flow boiling heat transfer in microchannels for thermal management with monolithically-integrated silicon nanowires, Nano Lett. 12 (2012) 3385–3390.
[33] C.C. Hsu, P.H. Chen, Surface wettability effects on critical heat flux of boiling heat transfer using nanoparticle coatings, Int. J. Heat Mass Transfer 55 (2012) 3713–3719.
[34] B. Feng, K. Weaver, G.P. Peterson, Enhancement of critical heat flux in pool boiling using atomic layer deposition of alumina, Appl. Phys. Lett. 100 (2012) 053120.
[35] J. Bico, U. Thiele, D. Quere, Wetting of textured surfaces, Colloids Surf., A 206 (2002) 41–46.
[36] K.Q. Peng, Y.J. Yan, S.P. Gao, J. Zhu, Synthesis of large-area silicon nanowire arrays via self-assembling nanoelectrochemistry, Adv. Mater. 14 (2002) 1164–1167.
[37] Z. Huang, N. Geyer, P. Werner, J. de Boor, U. Gösele, Metal-assisted chemical etching of silicon: a review, Adv. Mater. 23 (2011) 285–308.
[38] K.Q. Peng, Y. Wu, H. Fang, X.Y. Zhong, Y. Xu, J. Zhu, Uniform, axial-orientation alignment of one-dimensional single-crystal silicon nanostructure arrays, Angewandte Chemie-International Edition 44 (2005) 2737–2742.
[39] K.Q. Peng, Y.J. Yan, S.P. Gao, J. Zhu, Dendrite-assisted growth of silicon nanowires in electroless metal deposition, Adv. Funct. Mater. 13 (2003) 127–132.
[40] B.S. Kim, Boiling heat transfer enhancement by micro-nanoscale surface manipulation, Ph.D. Thesis, Yonsei University, 2011.
[41] A.F. Mills, Basic Heat and Mass Transfer, second ed., Prentice Hall, Upper Saddle River, N.J., 1999.
[42] F.P. Incropera, Fundamentals of Heat and Mass Transfer, sixth ed., John Wiley, Hoboken, N.J., 2007.
[43] V. Khanikar, I. Mudawar, T. Fisher, Effects of carbon nanotube coating on flow boiling in a micro-channel, Int. J. Heat Mass Transfer 52 (2009) 3805–3817.
[44] S.J. Kline, The purposes of uncertainty analysis, J. Fluids Eng. 107 (1985) 153–160.
[45] Y.Y. Hsu, On the size range of active nucleation cavities on a heating surface, J. Heat Transfer-Trans. ASME 84 (1962) 207–213.
[46] N. Basu, G.R. Warrier, V.K. Dhir, Onset of nucleate boiling and active nucleation site density during subcooled flow boiling, J. Heat Transfer-Trans. ASME 124 (2002) 717–728.
[47] Y.A. Dai, H.C. Chang, K.Y. Lai, C.A. Lin, R.J. Chung, G.R. Lin, J.H. He, Subwavelength Si nanowire arrays for self-cleaning antireflection coatings, J. Mater. Chem. 20 (2010) 10924–10930.
[48] N.Y. Zuber, Hydrodynamic aspects of boiling heat transfer, AEC, Report AECU-4439, 1959.
[49] I.G. Malenkov, Detachment frequency as a function of size for vapor bubbles, J. Eng. Phys. Thermophys. 20 (1971) 704–708.
[50] K.N. Rainey, S.M. You, Effects of heater size and orientation on pool boiling heat transfer from microporous coated surfaces, Int. J. Heat Mass Transfer 44 (2001) 2589–2599.
[51] J.S. Coursey, J. Kim, Nanofluid boiling: the effect of surface wettability, Int. J. Heat Fluid Flow 29 (2008) 1577–1585.
[52] Z. Yao, Y.W. Lu, S.G. Kandlikar, Effects of nanowire height on pool boiling performance of water on silicon chips, Int. J. Therm. Sci. 50 (2011) 2084–2090.